PCCP

Structural Insights into Self-Assembly of a Slow-Evolving and Mechanically Robust Supramolecular Gel via Time-resolved SANS

Journal:	*Physical Chemistry Chemical Physics*
Manuscript ID	CP-ART-04-2022-001826.R2
Article Type:	Paper
Date Submitted by the Author:	05-Nov-2022
Complete List of Authors:	Mirzamani, Marzieh; University of Cincinnati, James Winkle College of Pharmacy Dawn, Arnab; Wacker Chemical Corporation, Research and Development; Garvey, Christopher; Heinz Maier Leibnitz Centre He, Lilin; ORNL, Koerner, Hilmar; Air Force Research Laboratory Materials and Manufacturing Directorate, Composites Branch (RXCC) Kumari, Harshita; University of Cincinnati James L Winkle College of Pharmacy,

ARTICLE

Structural Insights into Self-Assembly of a Slow-Evolving and Mechanically Robust Supramolecular Gel via Time-resolved SANS

Received 00th January 20xx,
Accepted 00th January 20xx

DOI: 10.1039/x0xx00000x

Marzieh Mirzamani,[a†] Arnab Dawn,[a†] Christopher J. Garvey,[b] Lilin He,[c] Hilmar Koerner,[d] and Harshita Kumari*[a]

The supramolecular assembly process is a widespread phenomenon found in both synthetically engineered and naturally occurring systems, such as colloids, liquid crystals and micelles. However, a basic understanding of the evolution of self-assembly processes over the time remains elusive, primarily owing to the fast kinetics involved in these processes and the complex nature of the various non-covalent interacions operating simultaneously. With the help of a slow-evolving supramolecular gel derived from a urea-based gelator, we aim to capture the different stages of the self-assembly process commencing from nucleation. In particular, we are able to study the self-assembly in real time using time-resolved small-angle neutron scattering (SANS) at length scales ranging from approximately 30 Å to 250 Å. Systems with and without sonication are compared simultaneously, to follow the different kinetic paths involved in these two cases. Time-dependent NMR, morphological and rheological studies act complementarily to the SANS data at sub-micron and bulk length scales. A hollow columnar formation comprising of gelator monomers arranged radially along the long axis of the fiber and solvent in the core is detected at the very early stage of the self-assembly process. While sonication promotes uniform growth of fibers and fiber entanglement, the absence of such a stimulus helps extensive bundle formation at a later stage and at microscopic domain, making the gel system mechanically robust. The results of the present work provide a thorough understanding of the self-assembly process and reveals a path for fine-tuning such growth processes for applications such as the cosmetics industry, 3D printing ink development and paint industry.

Introduction

Supramolecular gelation is a fascinating representative self-assembly process that closely mimics important natural and biological events.[1-4] The supramolecular nature of such materials imparts the system with reversibility and adaptivity. The individual or collective contributions of various noncovalent interactions, such as hydrogen bonding, π–π stacking, metal–ligand coordination, host–guest interactions, and van der Waals interactions, are at the focal point of the structural evolution during an assembly process. Supramolecular gels have been studied extensively in the last few decades, mostly by exploiting the functional outputs for technological and medicinal applications.[5-21] An excellent example involves enabling use of an epoxy resin with thermo-activated organic thixotropes, where low-molecular weight diamide-based derivatives of hydroxystearic acid are shown to be thermally activated to facilitate direct writing of epoxy.[22] Another example entails utilizing scanning electron and X-ray microscopy to spatially control the cross-linking in a liquid polymer hydrogel solution on the nano- and micrometer scales, facilitating applications in tissue engineering and drug delivery.[23] Further examples can be found of carbohydrate-based low-molecular weight gelators (LMWGs) being applied to environmental remediation, 3D printing, ion sensing, catalysis, and drug delivery;[24] as well as exploring the molecular structures and rheological properties of LMWGs that make them suitable for use in 3D printing,[25] such as a gel with a UV-sensitive moiety permitting rapid curing with a robust structure[26] and an easily soluble gel that can used as a sacrificial ink.[27] By comparison, purely structural investigations of supramolecular gel materials during assembly are rather limited.[28-33] The lack of convincing structural data during formation of the gel/gel kinetics has multiple implications, especially controlling hierarchical self-assembly process of materials in aviation (3D printing). The two most crucial factors for structural investigations are the experimental time scale and the sensitivity of the measurements to different structural aspects during structural evolution. Therefore, the characterization of supramolecular gels is often considered far more challenging than the characterization of solution-phase materials.[34] Techniques like liquid state NMR, which are normally very sensitive to the local environment of a freely

[a] James L. Winkle College of Pharmacy, University of Cincinnati, 231 Albert Sabin Way, Cincinnati, OH 45267-0004, USA
[b] Heinz Maier-Leibnitz Zentrum (MLZ), Technische Universität München, Lichtenbergstraße 1, 85748 Garching, Germany
[c] Neutron Scattering Division, Oak Ridge National Laboratory, 1 Bethel Valley Rd., Oak Ridge, TN 37831, USA
[d] Materials & Manufacturing Directorate, Air Force Research Laboratory, WPAFB, Ohio 45433, United States
† Equal author contribution
*Corresponding author email: kumariha@ucmail.uc.edu

Electronic Supplementary Information (ESI) available: [^{1}H-NMR of **1** in DMSO-d_6, ESI mass spectra of **1**, molecular length calculation of hypothetically extended **1**, and details of SANS fitting results and scattering length density calculation.]. See DOI: 10.1039/x0xx00000x

tumbling molecule in solution, is dominated by signal broadening caused by shorter T_2 relaxation times. Electron microscopy, on the other hand, has issues associated with the artifacts caused by the solvent drying method. Similarly, rheological studies, which measures the bulk behavior of a system, cannot directly follow primary assembly process at the local scale of gel formation.

Typically, a stronger gel is considered superior to a weaker gel, and rapid gel formation makes the situation even more complex. Slowing down gel formation might provide an expanded time window for following the self-assembly process. However, control cannot be achieved over gel formation pathways involving sequential and/or continuous intermolecular assembly processes in space aided by various supramolecular interactions. Understanding the self-assembly process will give us the tools to control the process for the variety of applications discussed above. Classically, supramolecular gel formation involves multiple stages of assembly processes. Initially, when gelator molecules are homogenized (usually by a heat-triggered process) in a gel-forming solvent, nucleation occurs with time and/or temperature (by cooling down). In this process, monomeric molecules interact with each other noncovalently to arrange in specific directions, which can be considered as a primary assembly. Because of the molecular/chemical design of gelator molecules, in most of the cases, the primary assembly propagates in one dimension to form fibers, which are the structural backbone of supramolecular gel formation. However, simple fiber formation is not sufficient to hold the solvent molecules and attain the viscoelastic behavior of a gel. These characteristics can be achieved when the primary assemblies (typically fibers) undergo cross-linking in a supramolecular fashion (in the case of a supramolecular gel) to form a three-dimensional network structure in space. This entire event can occur within a minute or can take several hours, depending on the efficiency of the intermolecular interactions. To obtain insight into the gel formation event, the following issues need to be addressed: (i) whether single or multiple molecular stacks (fibers) are involved in the primary assembly process; (ii) how the fiber dimensions change during the secondary interaction (cross-linking); and (iii) whether formation of the primary and secondary assemblies occurs simultaneously or sequentially. Although there have been attempts to address some of these issues using various approaches,[28, 30, 33, 35] the absence of meaningful time-resolved data has limited the effort considerably.

In the present work, we aimed to explore some of the least studied aspects of supramolecular gel formation with the help of time-lapse experiments, primarily by using SANS technique. SANS is considered a powerful tool for elucidating structural information in substances at a mesoscopic scale ranging from 1 to 200 nm. In addition to the size, SANS can also provide accurate information about the shape of an assembly structure.[36-41] Advantageously, SANS experiments can be performed in the presence of solvent, allowing the solute–solvent interplay to be taken into the account. Some other advantages of SANS (especially over small-angle X-ray scattering (SAXS)) are the scope of isotope labeling and the nondestructive nature of neutrons. As this approach requires a relatively long gelation time to allow for the collection of time-resolved data, we attempted to design a supramolecular gel system in which the balanced intermolecular interactions can result in slow formation of primary and/or secondary assemblies, offering ample time to capture the nucleation process.

Here, our molecular design of **1** consists of three key elements: a hydrogen-bond forming urea motif, a stacking-interaction-forming aromatic motif, and a highly solubilizing tert-butyloxycarbonyl (BOC) group. Bisurea-based gelators are well-known for their tendency to form highly efficient one-dimensional assembly structures via cooperative urea tape formations at two points.[42-46] The presence of a single urea group, on the other hand, is expected to alter the assembly structure. Here, the presence of the BOC group plays a vital role by partially weakening the cooperative participation of intermolecular hydrogen bonding and stacking interactions. Further, the BOC group provides the necessary van der Waals interactions to initiate network formation via higher order assembly. Therefore, this molecular design balancing the interaction parameters is expected to offer an ideal platform for time-resolved studies of the assembly process. Indeed, **1** formed a transparent gel in chloroform (a gel formation was evaluated by stable-to-inversion method) and the gelation time could be extended to more than 10 h using a 1% (w/v) gelator concentration. However, sonicating the system during the initial stage shortened the gelation time considerably. Using SANS, the gel samples (sonicated and nonsonicated) were tested in low-q and high-q regions over a period of 8 h, to capture the nucleation event spanning different time scales. There are reports on the use of SANS to study supramolecular gel systems,[47-55] including ours.[56-58] However, to the best of our knowledge, this is the first report of a time-resolved SANS study on the nucleation behavior of a supramolecular gel system. Using SANS with complementary spectroscopy, rheology, and morphological investigations, the present study offers an important fundamental understanding of the kinetics and propagation of the self-assembly processes involved in supramolecular gelation.

Experimental

Synthesis of 1

1-(N-Boc-aminomethyl)-4-(aminomethyl)benzene (1 g, 4.2 mmol) was refluxed with benzyl isocyanate (0.6 g, 4.6 mmol) in 100 ml of anhydrous chloroform under a nitrogen atmosphere. The solvent was removed in vacuo and the crude product was purified by column chromatography [silica gel, CHCl3/MeOH = 15:1 (v/v)] to give a yellowish white powder (1.2 g, 77% yield). ^{1}H NMR (400 MHz, DMSO-d6): δ 1.39 (9H, s, –C(CH3)3), 4.12–4.24 (6H, m, ArCH2–NH–), 6.4 (2H, br, –CONHCH2Ar), 7.2–7.35 (9H, m, ArH). MS (ESI): m/z calcd. 369.2, found 392.2 [M + Na]+.

NMR Spectroscopy

NMR spectra ^{1}H were acquired on a Bruker AVANCE NEO-400 spectrometer using a single 30^o pulse of 14 μs duration. Each spectra was the result of 16 FID's with a relaxation delay of 1 s between pulses. The time dependent signal was then Fourier Transformed into the frequency domain.

Rheological Studies

Rheological studies were performed using a Discovery Hybrid Rheometer DHR-1 from TA Instruments. Gel samples of **1** were prepared in chloroform at room temperature and aged for 24 h before transferring to the rheometer plate, which was kept at 10 °C. A 40 mm steel cone plate geometry with 55 μm truncation was used for all experiments. Stress sweep experiments were performed at a constant frequency of 1 HZ, and frequency sweep experiments were performed at a constant strain of 0.5%.

SEM

Prepared gel samples of **1** were cast onto a silicon wafer, dried in vacuo for 2 days, and then coated with platinum. SEM images of the samples were obtained with a SCIOS SEM/FIB instrument.

SANS

The gel sample was prepared in $CDCl_3$ at a concentration of 2% (w/v) **1** to reduce the amount of incoherent scattering and to improve the contrast. The sample was heated using a heat gun until the gelator was completely dissolved. The hot solution was then injected into a pre-heated Helma cell of 2 mm pathlength using a heated needle and syringe to reduce the chance of gel formation during sample transfer. Once the cell holders were capped, one sample was sonicated for approximately 1 minute, while the other was left unsonicated. To best obtain an understanding of how the gel structure developed over a period of 8 hours just after homogenization, separate samples were prepared and measured for each instrument configuration. The SANS measurements were performed at 22 °C using the GP-SANS instrument (CG2) in the High Flux Isotope Reactor facility at Oak Ridge National Laboratory (Oak Ridge, TN, USA).[59] Two instrument configurations were used to yield an overall q range of 0.001 Å^{-1} < q < 0.23 Å^{-1}, where q = $(4\pi/\lambda)\sin(\theta/2)$ (q = scattering vector; λ = neutron wavelength; θ = scattering angle). The high-q configuration (0.0081 Å^{-1} < q < 0.23 Å^{-1}) used a neutron wavelength of λ = 4.75 Å and a sample-to-detector distance (SDD) of 6 m. The low q configuration (0.001 Å^{-1} < q < 0.019 Å^{-1}) used a neutron wavelength of λ = 12 Å and an SDD of 19.1 m. The wavelength distributions in both configurations were $\Delta\lambda/\lambda$ = 13%. Beginning 3 minutes after the samples were homogenized, a series of 5 minute scans were collected over a period of 8 hours at high-q and low-q. The raw counts on the area detector were converted to I(q) in Mantid[60] by first correcting for the dark current, empty cell scattering, and the sensitivity of the individual detector pixels, and then circular averaging the 2D data to obtain the 1D data. The reduced data were set to absolute scale by using porous silica as a secondary standard. The high- and low-q data were merged in IgorPro using macros developed by NIST.[61] The data were then fitted in SasView 5.0.3[62] with a smeared fractal core-shell cylinder model in order to account for the instrumental resolution.

Results and discussion

Gel Samples Studied

Gelator **1** gave transparent gels in chloroform. Gel formation (as evaluated by the stable-to-inversion method) was slow and took over 10 h for a concentration of 1% (w/v). To influence the kinetics of gel formation process, we adopted two different approaches for preparing the gel samples. In the first approach, we homogenized **1** in the solvent at a high temperature and then left the sample undisturbed at room temperature (RT, 20 °C) for nucleation and subsequent gel formation. In the second approach, after 30 min of mixing, we sonicated the homogenized system (sol) containing **1** for 1 min and then left the sample undisturbed at RT for nucleation and subsequent gelation. Interestingly, the sonicated system formed a gel in 3 h for a concentration of 1% (w/v). Sonication-induced gelation can be approximated as a rapid crystallization process that facilitates the formation of intermolecular interactions by suppressing and/or destroying any intramolecular interactions.[63] The presence of such an external stimulus is expected to influence first, the gelation kinetics, and second, the overall assembly behavior of **1**. Therefore, using the various characterization methods employed in this study, systems prepared with and without sonication were tested in parallel.

NMR, Rheology, and Morphology

^{1}H NMR is highly sensitive not only towards the molecular conformation, molecular mobility, translational diffusion and intermolecular interactions, offering qualitative valuable short range information about molecular assembly particularly in the early stages of assembly. The perspective offered here by a high resolution ^{1}H liquids NMR spectrometer and probe is on the monomers and smaller oligomers since efficient T_2 relaxation[64] precludes efficient detection of immobile protons due to probe deadtime effects. This effect has been used previously to provided kinetic detail of starch depolymerization,[65, 66] however in this discussion we restrict ourselves to qualitative observations around the behavior of monomers and small aggregates.

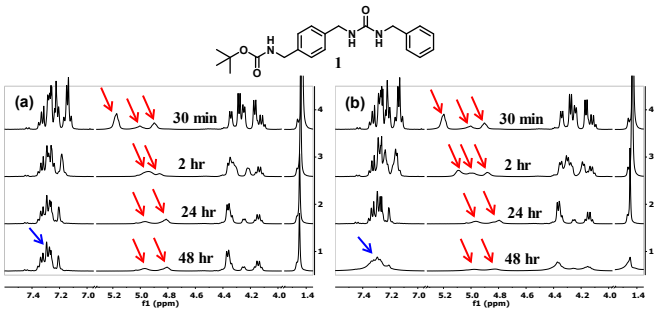

Figure 1 - Structure of **1** (top) and ^{1}H NMR spectra of **1** in $CDCl_3$ at various time intervals after homogenization: (a) nonsonicated and (b) sonicated (red and blue arrows indicate the signals associated with the protons linked to N and aromatic hydrogens, respectively).

Solvents like DMSO, which are strong hydrogen-bond accepters, inhibit molecular assembly by disfavoring the formation of intermolecular hydrogen bonds; thus, gelator molecules frequently exist as monomers in such solvent systems. Initially we assessed the various proton signals of **1** in the well-dispersed monomeric state in DMSO-d_6 (ESI, Figure S1). As expected, distinct and well-resolved signals were observed for all the protons, including the urea protons, signifying the absence of a molecular assembly. Next, to assess the assembly properties of **1**, we performed a series of single pulse ^{1}H NMR studies in a gel-forming solvent ($CDCl_3$) as the function of time and sonication (Figure 1). During the initial stage of gel formation, the NMR spectra associated with the sonicated and nonsonicated systems are very similar. Three signals appear in the range 4.7–5.2 ppm, these signals are ascribed to the two urea protons and the proton attached to nitrogen near the BOC group in **1**. With time these signals broaden and become less distinct. The broadening is most distinct and in the other resonances in the sonicated sample. This is consistent less of the oligomeric form in the gel formed from the sonicated solution. This differential behavior over DMSO-d_6 could be the result of either the increased presence of free molecules vs. more assembled molecules, or a conformational restriction of **1** gel-forming in $CDCl_3$. Either of these scenarios signifies a molecular assembly. Because of anticipated very fast T_2 relaxation in dense molecular assembly it is reasonable to consider that the observed signals are mostly coming from oligomeric species. However, continuous signal broadening over time still could be related to higher order assembly resulting in denser packing. Two additional physical effects that could lead to this effect includes more dipole interaction and chemical shift anisotropy. Surprisingly, the urea hydrogens exhibit an upfield shift, signifying a shielding event. It is possible that the nearby benzene ring adopts a conformation that brings it in close proximity to the urea hydrogen, inducing a shielding effect. This effect outweighs the conventional downfield shift caused by hydrogen-bonding interactions.[67] A comparison of the sonicated and nonsonicated systems reveals two important findings. First, the kinetics of assembly formation differ, as evidenced by the changes in the signals associated with different protons attached to nitrogen with time.

The differential effect of sonication on gel formation prompted us to study the rheology of the associated systems. To minimize solvent loss during the rheological studies, experiments were performed using chloroform gels of **1** (2%, w/v) at 10 °C. While all the tested gel systems of **1** exhibit extremely high mechanical strength, the stress sweep experiment reveals that the nonsonicated system has a higher storage modulus and yield stress than the sonicated system (Figure 2a). Therefore, the sonication stimuli can significantly affect the higher order assembly such as entanglement and bunding of fibers. A practically frequency-independent moduli with G′ >> G′′, on the other hand, signifies a stable assembly structure over the examined time scale for both the sonicated and nonsonicated systems (Figure 2b).

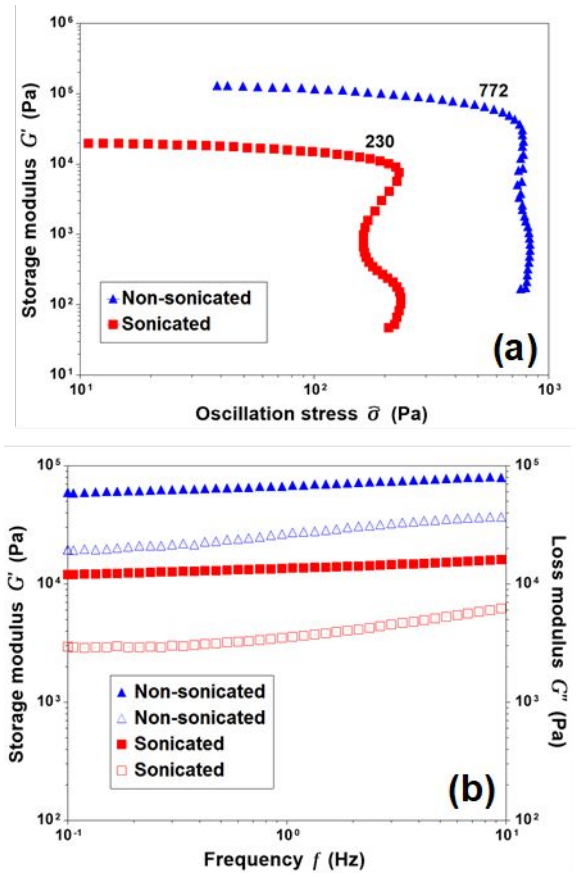

Figure 2 - Rheology of sonicated and nonsonicated gels of **1** in $CDCl_3$ (2%, w/v) at 10 °C: (a) stress sweep experiments at a constant frequency of 1 Hz (yield stress values are indicated), and (b) frequency sweep experiments at a constant strain of 0.5% (filled and empty symbols correspond to G′ and G′′, respectively).

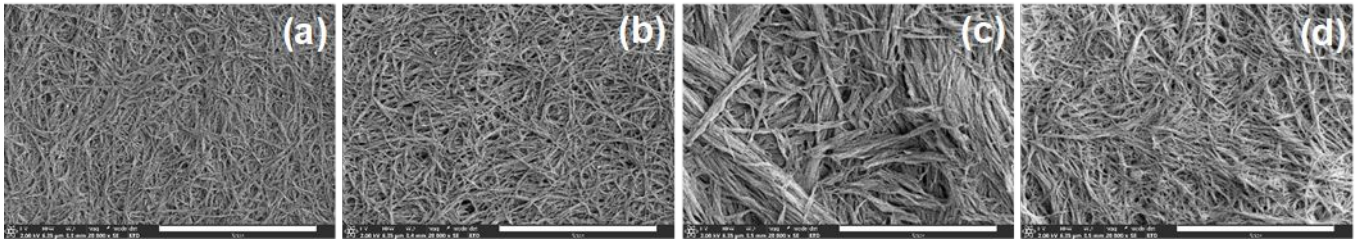

Figure 3 - SEM images of nonsonicated and sonicated gels of **1** in $CDCl_3$ prepared at different time intervals after homogenizing: (a) nonsonicated gel after 30 min, (b) sonicated gel after 30 min, (c) nonsonicated gel after 24 h, and (d) sonicated gel after 24 h. The scale bars represent 3 μm.

To obtain insight into the morphology of the above systems, scanning electron microscopy (SEM) was performed on the gel samples of **1** at the initial and final stages of gel formation. In general, the morphology of the gel systems was fibrous with some finer differentiations observed as functions of time and sonication. At the initial stage, the fibrous structures of the sonicated and nonsonicated gels are practically the same with similar fiber thicknesses (Figure 3a and 3b). However, after complete gel formation (over 24 h), there are significant differences in the fiber structures (Figure 3c and 3d). First, the fiber dimensions show remarkable uniformity in the sonicated system, whereas the nonsonicated system exhibits a wide distribution of fiber dimensions. Second, bundling of fibers is very prominent in the absence of sonication. In the sonicated system, the fibers also become thicker, but to a lesser extent and without losing the uniformity in distribution. This preferential fiber bundling might explain the high mechanical strength of the nonsonicated system in the rheological study (Figure 2).

Time-Resolved SANS Study

SANS measurements were done on sonicated and nonsonicated gels formed in $CDCl_3$. SANS provides structural perspectives over a broad range of length-scales in reciprocal space, characterized by the scattering vector q, where $q= (4\pi/\lambda)\sin(\theta)$ and λ is the wavelength of the scattered radiation and 2θ is the scattering angle. SANS measurements were made at two instrument configurations where the low q region corresponds to a longer length scale and the high q corresponds to a shorter length scale. The low-q and high-q regions for both gels were each measured over a period of 8 h using a series of 5 min acquisitions. Since a fresh gel sample was made before each measurement to ensure that little to no gel structure had formed before the first SANS scan, we assume a matching time course for each gel measurement allowing us to follow how the entire gel structure formed after homogenization. The high-q scans spanned a q-range of 0.0081-0.23 $Å^{-1}$ (corresponding to a length scale of ~30-700 Å) while the low-q scans covered a q-range of 0.0010-0.019 $Å^{-1}$ (length scale of ~350-3500 Å); combined, the full-q ranges from 0.001 to 0.23 $Å^{-1}$.

SANS curve overlays for the non-sonicated gel and the sonicated gel and their fits using a fractal core-shell cylinder model are shown in Figure 4, and fits to the full q-range are shown in Figure S5 of the ESI. Other models were attempted, such as fractal flexible cylinder, lamellar models, and empirical models, but those were not able to sufficiently fit the combination of low-q slope and intensity and Bessel oscillations with two maxima at q= 0.05 $Å^{-1}$ and q= 0.1 $Å^{-1}$. A noticeable difference can be observed in the maximum at q = 0.05 $Å^{-1}$ for the nonsonicated and sonicated gels: it is broader in the nonsonicated gel, suggesting a more polydispersed structure; additionally, the scattering intensity of the maximum is more intense for the nonsonicated gel, indicating that there is a greater amount of the repeating structure contributing to the maximum. The position of this maximum remains consistent for the entire duration of the experiment and is the same for both the non-sonicated and sonicated gels, indicating that the repeating structure contributing to this maximum does not change significantly over time.

The data were fitted with a smeared fractal core-shell cylinder model. In other words, this model consists of the fractal structure factor from Teixeira[68] with the form factor of the core-shell cylinder model[69] replacing that of a solid sphere. The general equation describing the 1D scattering intensity consisting of a structure factor and a form factor is [68]

$$I(q) = P(q)S(q) + \text{background}$$

where *P(q)* is the form factor, *S(q)* is the structure factor and "background" is the level of incoherent scattering. The fractal structure factor is

$$S(q) = 1 + \frac{D_f\Gamma(D_f-1)}{[1+\frac{1}{(q\xi)^2}]^{(D_f-1)/2}} \frac{\sin[(D_f-1)\tan^{-1}(q\xi)]}{(qr_t)^{D_f}}$$

where D_f is the fractal dimension, ξ is the correlation length, and r_t is the total radius of the core-shell cylinder (i.e. core + shell thickness). For randomly oriented cylinders, the form factor is

$$P(q) = \frac{\text{scale}}{V_t}\int_0^{\frac{\pi}{2}} F^2(q,\alpha)\sin\alpha \mathrm{d}\alpha + \text{background}$$

where

$$F(q,\alpha) = (\rho_c-\rho_s)V_c\frac{\sin\left(q\frac{1}{2}L\cos\alpha\right)}{q\frac{1}{2}L\cos\alpha}\frac{2J_1(qr_c\sin\alpha)}{qr_c\sin\alpha} + (\rho_s-\rho_{solv})V_t\frac{\sin\left(q\left(\frac{1}{2}L+\right.\right.}{q\left(\frac{1}{2}L+T\right.}$$

and

$$V_t = \pi r_t^2(L+2T)$$

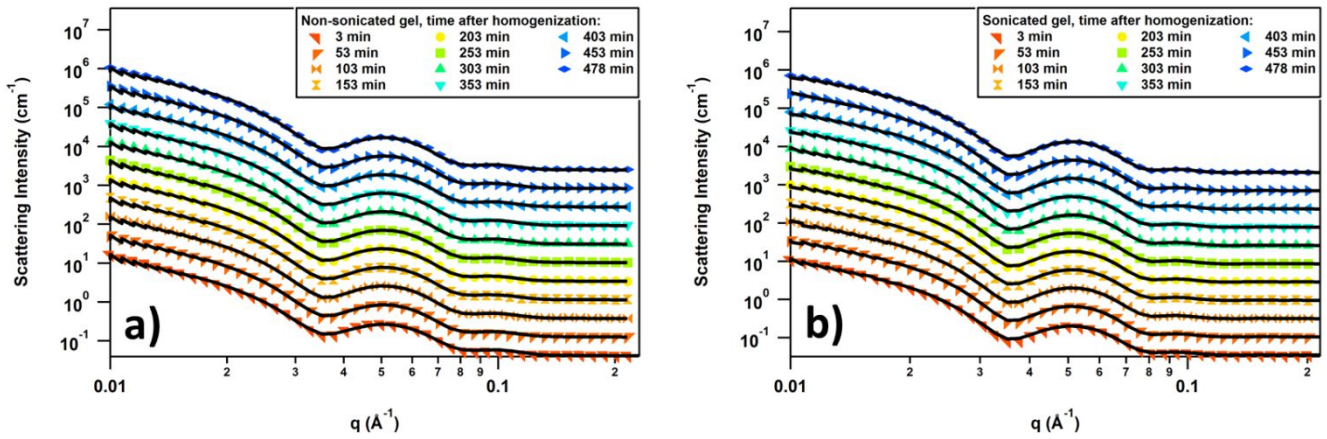

Figure 4 - SANS curves of a) the nonsonicated gel and b) the sonicated gel of 1 in deuterated chloroform at a concentration of 2 w/v% showing the fits to the data over the full q-range using a fractal core-shell cylinder model (solid black lines). All curves are offset by powers of 3 for visual clarity.

and α is the angle between the axis of the cylinder and $\vec{q}$, V_t is the total volume of the core-shell cylinder, V_c is the volume of the core, r_c is the radius of the core, L is the length of the core, T is the shell thickness, J_1 is the first-order Bessel function, and ρ_c, ρ_s, and ρ_{solv} are the scattering length densities of the core, the shell, and the solvent respectively.

The parameters—i.e. the volume fraction, core radius, shell thickness, polydispersity of the shell thickness, and fiber length—are plotted as a function of time for both types of gels in Figure 5. A number of differences between the two gels can be seen in the volume fraction (Figure 5a): 1) the volume fraction for the sonicated gel increased over time while the volume fraction for the nonsonicated gel decreased slightly over time, 2) the sonicated gel equilibrated approximately 50 min after homogenization whereas the nonsonicated gel needed 100 min to equilibrate, and 3) the volume fraction for the nonsonicated gel was about 50% greater than that of the sonicated gel (0.015 for nonsonicated gel vs. 0.01 for sonicated gel). Both were less than the calculated volume fraction determined from the concentration of the sample (2 wt/v%) and the molecular volume calculated with MULCh,[70] indicating that a portion of the gelator in each system remained dissolved in its monomeric state. Furthermore, this means that more of the gelator in the nonsonicated gel (approximately 64%) participated in the formation of the gel structure compared to the sonicated gel (approximately 42%), and thus the nonsonicated gel system has more structure than the sonicated gel system. The thickness of the shell (Figure 5b) increased over time for both gels before equilibrating after 50 min for the sonicated gel and 100 min for the nonsonicated gel, with the shell of the sonicated gel fiber being approximately 25% thicker than that of the nonsonicated gel (50 Å vs. 40 Å, respectively). The shell of the sonicated gel fibers was also very monodisperse compared to that of the nonsonicated gel fiber (0.05 vs. 0.225), with similar equilibration times, as shown in Figure 5c. Despite the time needed to equilibrate, however, the shell thicknesses did not increase substantially, indicating that the shell structure was mostly formed immediately after homogenization. The core radius values in Figure 5d show the same equilibration times as the volume fraction and shell thickness equilibration times for both gels, except the core radius values decrease slightly over time while the volume fraction and shell thickness values increase over time. When considered with the changes in the shell thickness over time, it further indicates that the full core-shell geometry is formed soon after homogenization. Additionally, the core radius of the nonsonicated gel is about 5 Å larger than that of the sonicated gel. The overall radius of the sonicated gel fiber (core radius + shell thickness) is still larger than that of the nonsonicated gel fiber, with an overall radius of 92 Å vs. 87 Å, respectively. Interestingly, the overall diameter of these fibers as well as the shell thickness are much larger than the length of **1** if it were hypothetically fully extended (ESI, Figure S3). Although the number of gelator molecules surrounding the core cannot be determined, the gelators may arrange themselves via π-π stacking and H-bonding to form the core-shell cylinder structure as shown in Figure 6. Based on the shell thickness values, it appears that the gelator arrangement is affected by the effect of sonication, such that the gelators in the nonsonicated gel arrange themselves end-to-end to achieve the 40 Å shell thickness, while the gelators in the sonicated gel arrange themselves in an offset, antiparallel double layer to reach a shell thickness of 50 Å. These arrangements also explain the core-shell geometry, as the lipophilic *tert*-butyl ends face toward the solvent, thus allowing the hydrophilic urea groups to remain inside the fiber away from the solvent. Finally, the fiber lengths (Figure 5e) for both the nonsonicated and sonicated gels surprisingly took about 100 min to equilibrate, with the sonicated gel fibers being approximately 50% longer than the nonsonicated gel fibers (1650 Å vs. 1100 Å, respectively). The fractal dimension as a function of time is shown in the ESI (Figure S4), which indicates the different network structures formed in the two gels.

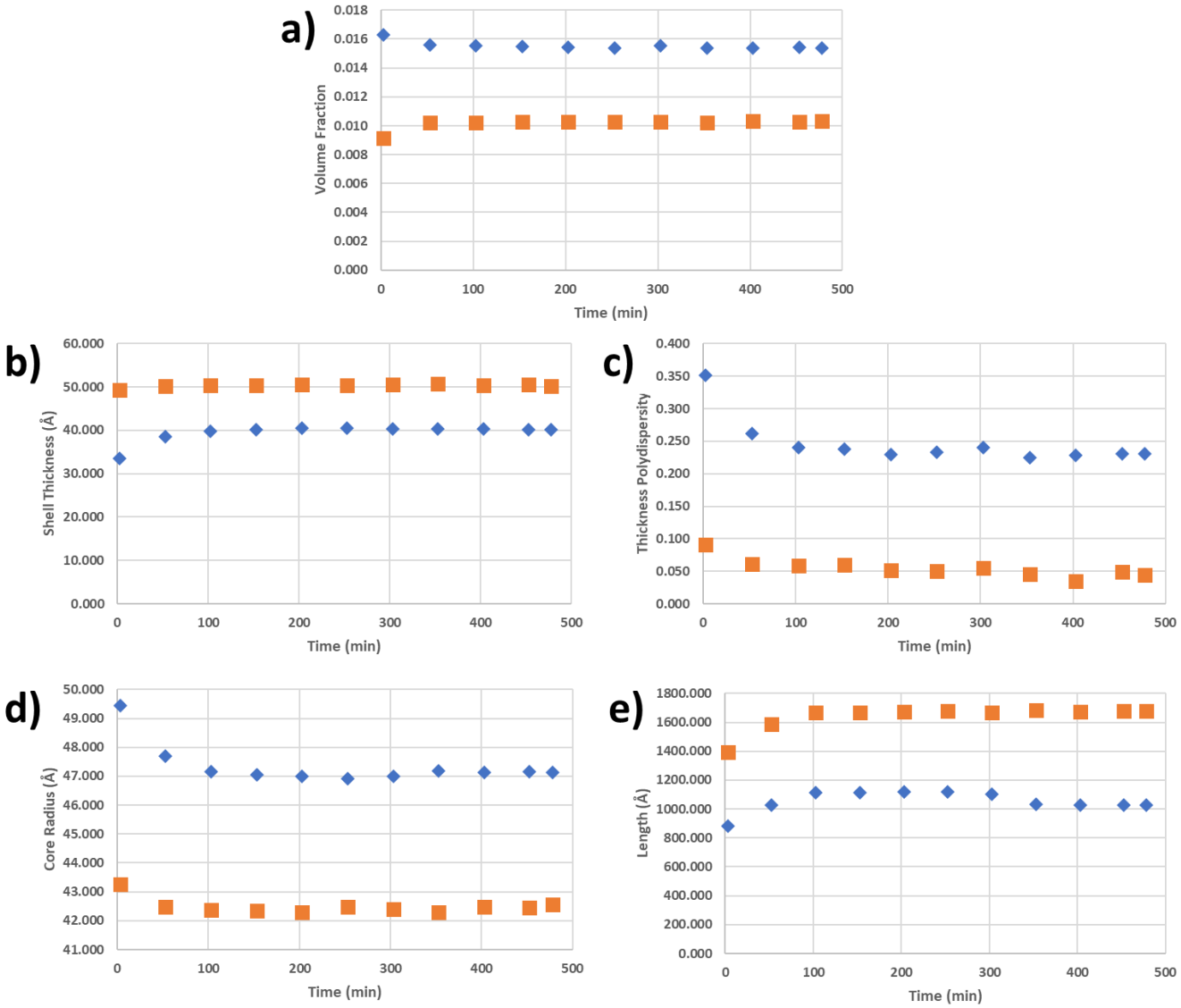

Figure 5 - The volume fraction (a), shell thickness (b), polydispersity of the shell (c), the core radius (d), and cylinder length (e) values over time after homogenization as determined from the SANS modeling (error bars are too small to be distinguished from the symbols). The blue diamonds are the results for the non-sonicated gel, whereas the orange squares are the sonicated gel results.

Despite the difference in macroscopic gelation times for sonicated and nonsonicated gels (3 h vs 12 h), each system equilibrates after about 50 min and 100 min, respectively. However, the nonsonicated gel shows more noticeable changes occurring over that somewhat longer period of time compared to the sonicated gel, showing that the stimulus affected the interactions between the gelator molecules and thereby influenced the final structure of the fully formed gel. The differential behaviors in bulk property, on the other hand, originate mainly from the secondary assembly comprising of fiber bundling, fiber entanglement etc.

Structural Analysis

From the time-resolved experiments supported by the NMR, morphology, and rheology data, a few conclusions can be drawn unambiguously: (i) the overall assembly patterns including the hierarchy are quite similar for the gels in presence and in absence of sonication; (ii) the structural evolution differs mostly in first 100 mins for sonicated and nonsonicated gels; (iii) the structural evolution with time is more consistent for sonicated system; (iv) polydispersity in ordered structures is more prominent in the nonsonicated system; and (v) higher order structure (bundling and entanglement) are more abundant in the nonsonicated gel. Thus, there are two key areas of interest: the structural evolution of each type of system, and their comparative natures in presence and in absence of the stimulus. It should be noted that the time-lapse SANS study specifically addresses the local growth processes occurring on the short length scale (high q region), as the resolution is not high enough to draw conclusions from the processes occurring on longer length scales. In contrast, morphology and rheology can take long-range interactions into account. ^{1}H NMR, on the other hand, can capture both domains but with limited finer detail. As the primary assembly structure of a supramolecular

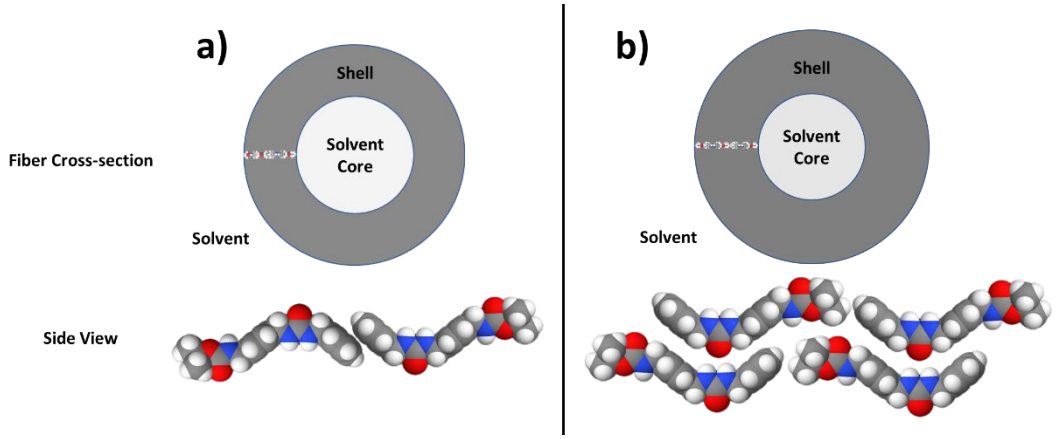

Figure 6 - Fiber cross-section across the long axis (top row) and side view (bottom row) showing the gelator arrangement inside the shell of the nonsonicated (a) and sonicated (b) fibers.

gel relies on the chemical structure of the gelator and the solvent system, it is expected that both the sonicated and nonsonicated systems will follow similar nucleation paths. Indeed, there is no striking difference between the two systems in terms of the assembly pattern (in this case, fiber formation). At the primary stage of nucleation, one expects the growth of a one-dimensional assembly of **1** via intermolecular hydrogen bonding (urea groups) and stacking interactions (aromatic groups). The overall fiber radius (core radius + shell thickness) obtained from SANS data indicates that the fibers are several folds thicker than hypothetically stretched **1** (ESI, Figure S3), which is indicative of a core-shell cylinder geometry of the fiber, where the gelator monomers are arranged in the shell while the solvent is within the core and surrounding the cylinder (Figure 7b). This result is quite significant because even though the gel formation is quite slow, primary cluster formation occurs within the first 50 min in the sonicated gel and within the first 100 min in the nonsonicated gel, as evident from SANS data. The presence of a tertiary butyl group at one end of **1** might facilitate van der Waals interactions in a direction perpendicular to the one-dimensional growth axis, or enable the core-shell geometry by acting as the lipophilic group. This core-shell fibril arrangement is probably responsible for the extremely high mechanical strength of the gels. A quick and consistent levelling of core radius, shell thickness and fiber length (columnar fibers in the true sense) for the sonicated system indicates a more organized hierarchical event in presence of the mechanical stimuli (sonication) at the expense of the number of fiber bundles formed. Notably, the intermediate core-shell assembly structure is fairly uniform in shell thickness, as evident from the SANS fitting results (Figure 5c). This result supports the formation of a hollow columnar structure comprising defined numbers of gelator monomers in the shell oriented perpendicularly to the long axis of the columnar structure, as shown in Figure 6. At the local scale, we observed quite different growth kinetics for the sonicated and nonsonicated systems, however, the difference between values of a specific parameter (as summarized in Figure 5) for sonicated and non-sonicated system are never nullified. Therefore, the effect of the mechanical stimulus becomes more crucial than the time. Clearly, sonication helps disperse the assemblies uniformly from a random aggregated state. Furthermore, sonication helps achieve structural orderliness. Finally, sonication initiates quick core-shell formation at local scale by efficient intermolecular interaction. The same is also reflected in more prominent aromatic stacking in the sonicated gel, as indicated by the severe broadening of the associated aromatic signals in the NMR spectrum (Figure 1b). However, at the same time, sonication minimizes random interactions among the fibril clusters, thereby eliminating extensive bundling at microscopic domain as evident from SEM images of the fully matured gels (Figure 3c and 3d). Interestingly, the structurally less ordered nonsonicated gel appeared mechanically more robust (Figure 2a) because of the formation of higher order bundles especially at microscopic domain, as visualized by SEM (Figure 3c). These key findings are illustrated in Figure 7.

The different characterization methods employed here provided independent, valuable, and complementary information. NMR spectroscopy which works primarily in the molecular domain with the reflection of supramolecular events in cases, followed the formation of assemblies over time without finer differentiation between primary and secondary assemblies. SANS provided unprecedented insight into the local assembly structures and their evolution with time. In addition, SANS revealed the presence of polydispersity in the nonsonicated system. It is found that sonication helps to organize the structure from very early stage periodically and consistently over time. It is worth noticing that the formation of primary assembly is not only sonication independent but also completes within about 100 mins, while macroscopic properties keep changing until about 10 h. Therefore, such stimuli would be more influential towards the bulk behavior of the samples rather than early nucleation. Adopting a monodisperse assembly with the help of sonication by inhibiting extensive bundling could be crucial in the development of functional gels in which structural orderliness could amplify the functional output. In contrast, as revealed by SEM and rheological studies, bundle formation at the later stages of gelation improved the mechanical strength, which is beneficial for many biomedical applications. Therefore, the present study not only offers an unprecedented insight into the time-resolved phenomenon of supramolecular gel formation process but also provides

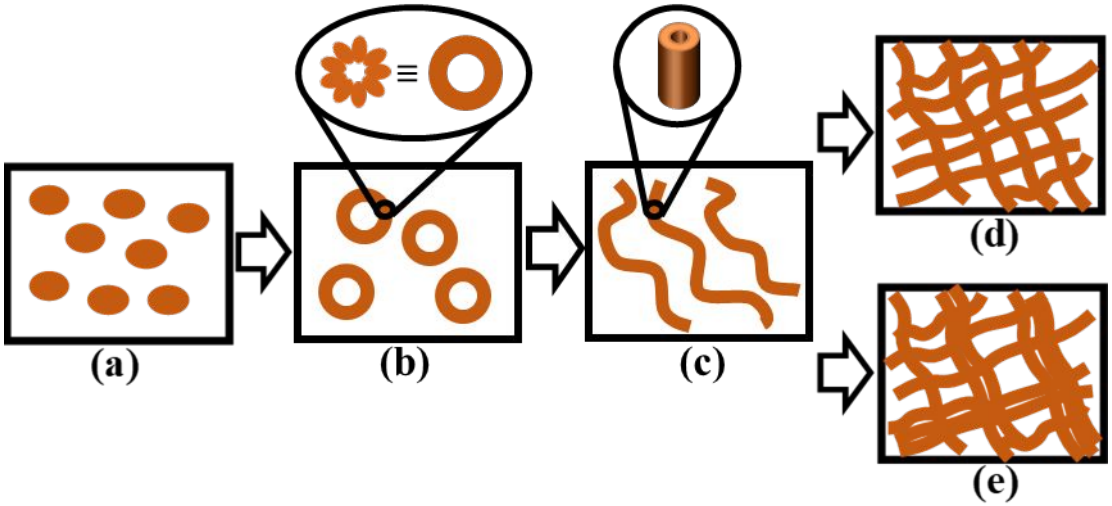

Figure 7 - Simplified illustrations of different stages of gel formation: (a) well-dispersed **1** in monomeric form immediately after homogenizing the substrate with the solvent, (b) intermediate molecular core-shell formation, trapping solvent within the formation, (c) stacks of molecular core-shell formations to form a hollow columnar structure, (d) uniformly distributed cross-linked assembly structure in the sonicated gel, and (e) polydispersity in the randomly distributed cross-linked assembly structure in the nonsonicated gel, which contains higher order (bundled) structures.

important information for programming the functional applications of a gelator.

Conclusions

In conclusion, the present work uses a slow-evolving supramolecular gel derived from a bis-urea gelator, in presence and in absence of sonication as the stimulus, to capture time-lapsed structural insights at various domains ranging from nanoscopic to microscopic scales. Time-lapse SANS experiments capture the quick formation of primary assembly composed of the core-shell arrangement of monomers within the shell and solvent in the core and then of stacking to form hollow columnar fibers, where the sonicated system is found to be more monodisperse in the shell thickness but less abundant in nature in terms of overall gel structure. Sonication induces a periodic and consistent growth and hierarchy in the assembly process at the local scale with time, which practically levelled after 50-100 mins irrespective of the stimulus. While sonication favors entanglement at local scale, in absence of such a stimulus, the gel structure of the nonsonicated system is formed with a majority of the gelator in the system and undergoes extensive and random bundling at microscopic domain as captured from SANS, NMR, morphological and rheological studies. This could be the reason behind the greater mechanical strength of the nonsonicated system compared to the sonicated system. The information provided by the present work will help to develop an in-depth understanding of supramolecular hierarchical assembly processes and their stimuli responsiveness together with the associated structure–function relationships, connecting the molecular level to the macroscopic level. This understanding can then be applied to tune the assembly processes of prospective gelators to produce faster curing or more robust 3D printing inks, controlling 3D printing in aviation applications, more effective scaffolds for tissue engineering, or to identify the best stage of gel assembly for efficient loading of a drug into the gel for drug delivery.

Author Contributions

MM: Conceptualization, Investigation, Formal analysis, Visualization, Writing—original draft, Writing—review and editing; AD: Conceptualization, Investigation, Formal analysis, Visualization, Writing—original draft, Writing—review and editing; CJ: Validation, Writing—review and editing; LH: Investigation, Validation, Writing—review and editing; HKo: Writing—review and editing; HKu: Funding, Conceptualization, Supervision, Writing—review and editing.

Conflicts of interest

There are no conflicts to declare.

Acknowledgements

The current work was funded through start-up funds provided by CoP, UC (HK). A portion of this research used resources at the High Flux Isotope Reactor, a DOE Office of Science User Facility operated by the Oak Ridge National Laboratory. This work benefited from the use of the SasView application, originally developed under NSF Award DMR-0520547. SasView also contains code developed with funding from the EU Horizon 2020 programme under the SINE2020 project Grant No 654000.

Notes and references

1. B. J. G. E. Pieters, M. B. van Eldijk, R. J. M. Nolte and J. Mecinović, *Chemical Society reviews*, 2016, **45**, 24-39.

2. W. Du, X. Hu, W. Wei and G. Liang, *Bioconjugate Chemistry*, 2018, **29**, 826-837.
3. Y. Bai, Q. Luo and J. Liu, *Chemical Society Reviews*, 2016, **45**, 2756-2767.
4. F. Chiti and C. M. Dobson, *Annual review of biochemistry*, 2017, **86**, 27-68.
5. P. Terech and R. G. Weiss, *Chem. Rev.*, 1997, **97**.
6. N. M. Sangeetha and U. Maitra, *Chem. Soc. Rev.*, 2005, **34**.
7. M.-O. M. Piepenbrock, G. O. Lloyd, N. Clarke and J. W. Steed, *Chem. Rev.*, 2010, **110**.
8. A. Dawn, T. Shiraki, S. Haraguchi, S. Tamaru and S. Shinkai, *Chem. Asian J.*, 2011, **6**.
9. L. E. Buerkle and S. J. Rowan, *Chem. Soc. Rev.*, 2012, **41**.
10. S. S. Babu, V. K. Praveen and A. Ajayaghosh, *Chemical Reviews*, 2014, **114**, 1973-2129.
11. Y. Feng, Y. M. He and Q. H. Fan, *Chemistry – An Asian Journal*, 2014, **9**, 1724-1750.
12. L. Zhang, X. Wang, T. Wang and M. Liu, *Small*, 2015, **11**, 1025-1038.
13. B. O. Okesola and D. K. Smith, *Chemical Society Reviews*, 2016, **45**, 4226-4251.
14. C. D. Jones and J. W. Steed, *Chem. Soc. Rev.*, 2016, **45**.
15. S. Bhattacharya and S. K. Samanta, *Chemical Reviews*, 2016, **116**, 11967-12028.
16. W. Fang, Y. Zhang, J. Wu, C. Liu, H. Zhu and T. Tu, *Chemistry, an Asian journal*, 2018, **13**, 712-729.
17. A. Dawn, *International Journal of Molecular Sciences*, 2019, **20**.
18. F. Fages and K. Araki, *Low molecular mass gelators : design, self-assembly, function*, Springer, Berlin ; New York, 2005.
19. R. G. Weiss and P. Terech, *Molecular gels : materials with self-assembled fibrillar networks*, Springer, Dordrecht, 2006.
20. B. Escuder and J. F. Miravet, *Functional molecular gels*, Royal Society of Chemistry, Great Britain, 2013.
21. A. Dawn, B. Roy and S. Shinkai, in *Chemoresponsive Materials : stimulation by chemical and biological signals*, ed. H.-J. Schneider, Royal Society of Chemistry, 2015, pp. xxvi, 529 pages.
22. R. McKenzie and H. Koerner, *Additive Manufacturing*, 2020, **31**.
23. T. Gupta, E. Strelcov, G. Holland, J. Schumacher, Y. Yang, M. B. Esch, V. Aksyuk, P. Zeller, M. Amati, L. Gregoratti and A. Kolmakov, *ACS Nano*, 2020, **14**, 12982-12992.
24. J. Morris, J. Bietsch, K. Bashaw and G. Wang, *Gels*, 2021, **7**, 24.
25. M. C. Nolan, A. M. Fuentes Caparrós, B. Dietrich, M. Barrow, E. R. Cross, M. Bleuel, S. M. King and D. J. Adams, *Soft Matter*, 2017, **13**, 8426-8432.
26. Z. Zhou, M. Samperi, L. Santu, G. Dizon, S. Aboarkaba, D. Limón, C. Tuck, L. Pérez-García, D. J. Irvine, D. B. Amabilino and R. Wildman, *Materials & Design*, 2021, **206**, 109792.
27. A. Chalard, M. Mauduit, S. Souleille, P. Joseph, L. Malaquin and J. Fitremann, *Additive Manufacturing*, 2020, **33**, 101162.
28. A. Dawn and H. Kumari, *Chem. Eur. J.*, 2018, **24**.
29. A. Dawn, T. Shiraki, H. Ichikawa, A. Takada, Y. Takahashi, Y. Tsuchiya, T. N. Lien le and S. Shinkai, *J Am Chem Soc*, 2012, **134**, 2161-2171.
30. W. Weng, J. B. Beck, A. M. Jamieson and S. J. Rowan, *Journal of the American Chemical Society*, 2006, **128**, 11663-11672.
31. Y. Zhang and R. G. Weiss, *Journal of colloid and interface science*, 2017, **486**, 359-371.
32. V. Ajay Mallia and R. G. Weiss, *Soft matter*, 2016, **12**, 3665-3676.
33. M. Yan, S. K. P. Velu, M. Maréchal, G. Royal, J. Galvez and P. Terech, *Soft matter*, 2013, **9**, 4428-4436.
34. G. Yu, X. Yan, C. Han and F. Huang, *Chem. Soc. Rev.*, 2013, **42**.
35. N. Nonappa and E. Kolehmainen, *Soft Matter*, 2016, **12**, 6015-6026.
36. M. J. Hollamby, K. Aratsu, B. R. Pauw, S. E. Rogers, A. J. Smith, M. Yamauchi, X. Lin and S. Yagai, *Angewandte Chemie International Edition*, 2016, **55**, 9890-9893.
37. J. P. Patterson, E. G. Kelley, R. P. Murphy, A. O. Moughton, M. P. Robin, A. Lu, O. Colombani, C. Chassenieux, D. Cheung, M. O. Sullivan, T. H. Epps and R. K. O'Reilly, *Macromolecules*, 2013, **46**, 6319-6325.
38. H. Fukuda, A. Goto and T. Imae, *Langmuir*, 2002, **18**, 7107-7114.
39. C. Malardier-Jugroot, T. G. M. van de Ven, T. Cosgrove, R. M. Richardson and M. A. Whitehead, *Langmuir*, 2005, **21**, 10179-10187.
40. H. Kumari, S. R. Kline, D. A. Fowler, A. V. Mossine, C. A. Deakyne and J. L. Atwood, *Chemical Communications*, 2014, **50**, 109-111.
41. H. Kumari, S. R. Kline, N. J. Schuster, C. L. Barnes and J. L. Atwood, *Journal of the American Chemical Society*, 2011, **133**, 18102-18105.
42. J. van Esch, R. M. Kellogg and B. L. Feringa, *Tetrahedron letters*, 1997, **38**, 281-284.
43. J. van Esch, S. De Feyter, R. M. Kellogg, F. De Schryver and B. L. Feringa, *Chemistry – A European Journal*, 1997, **3**, 1238-1243.
44. M. Yamanaka, *Journal of Inclusion Phenomena and Macrocyclic Chemistry*, 2013, **77**, 33-48.
45. J. W. Steed, *Chemical Society Reviews*, 2010, **39**, 3686-3699.
46. E. Yashima, N. Ousaka, D. Taura, K. Shimomura, T. Ikai and K. Maeda, *Chemical Reviews*, 2016, **116**, 13752-13990.
47. P. Terech, D. Pasquier, V. Bordas and C. Rossat, *Langmuir*, 2000, **16**.
48. P. Terech, A. Coutin and A. M. Giroud-Godquin, *J. Phys. Chem. B*, 1997, **101**.
49. M. George, G. P. Funkhouser, P. Terech and R. G. Weiss, *Langmuir*, 2006, **22**.
50. P. Terech, E. Ostuni and R. G. Weiss, *J. Phys. Chem.*, 1996, **100**, 3759-3766.
51. R. A. Hule, R. P. Nagarkar, A. Altunbas, H. R. Ramay, M. C. Branco, J. P. Schneider and D. J. Pochan, *Faraday Discuss.*, 2008, **139**.
52. A. R. Hirst, J. F. Miravet, B. Escuder, L. Noirez, V. Castelletto, I. W. Hamley and D. K. Smith, *Chemistry : a European journal*, 2009, **15**, 372-379.
53. A. R. Hirst, I. A. Coates, T. R. Boucheteau, J. F. Miravet, B. Escuder, V. Castelletto, I. W. Hamley and D. K. Smith, *Journal of the American Chemical Society*, 2008, **130**, 9113-9121.
54. I. W. Hamley, S. Burholt, J. Hutchinson, V. Castelletto, E. Rodrigo da Silva, W. Alves, P. Gutfreund, L. Porcar, R. Dattani, D. Hermida-Merino, G. Newby, M. Reza, J. Ruokolainen and J. Stasiak, *Biomacromolecules*, 2017, **18**.

55. P. Terech, I. Furman and R. G. Weiss, *J. Phys. Chem.*, 1995, **99**, 9558-9566.
56. A. Dawn, M. Mirzamani, C. D. Jones, D. S. Yufit, S. Qian, J. W. Steed and H. Kumari, *Soft Matter*, 2018, **14**, 9489-9497.
57. H. Kumari, S. E. Armitage, S. R. Kline, K. K. Damodaran, S. R. Kennedy, J. L. Atwood and J. W. Steed, *Soft Matter*, 2015, **11**.
58. H. Kumari, S. R. Kline, S. R. Kennedy, C. Garvey, C. L. Raston, J. L. Atwood and J. W. Steed, *Chem. Commun.*, 2016, **52**.
59. W. T. Heller, M. J. Cuneo, L. M. Debeer-Schmitt, C. Do, L. He, L. Heroux, K. C. Littrell, S. V. Pingali, S. Qian, C. B. Stanley, V. S. Urban, B. Wu and W. Bras, *Journal of Applied Crystallography*, 2018, **51**, 1-7.
60. O. Arnold, J. C. Bilheux, J. M. Borreguero, A. Buts, S. I. Campbell, L. Chapon, M. Doucet, N. Draper, R. Ferraz Leal, M. A. Gigg, V. E. Lynch, A. Markvardsen, D. J. Mikkelson, R. L. Mikkelson, R. Miller, K. Palmen, P. Parker, G. Passos, T. G. Perring, P. F. Peterson, S. Ren, M. A. Reuter, A. T. Savici, J. W. Taylor, R. J. Taylor, R. Tolchenov, W. Zhou and J. Zikovsky, *Nuclear Instruments and Methods in Physics Research Section A: Accelerators, Spectrometers, Detectors and Associated Equipment*, 2014, **764**, 156-166.
61. S. R. Kline, *J. Appl. Crystallogr.*, 2006, **39**, 895-900.
62. M. Doucet, J. H. Cho, G. Alina, Z. Attala, J. Bakker, W. Bouwman, P. Butler, K. Campbell, T. Cooper-Benun, C. Durniak, L. Forster, M. Gonzales, R. Heenan, A. Jackson, S. King, P. Kienzle, J. Krzywon, T. Nielsen, L. O'Driscoll, W. Potrzebowski, S. Prescott, R. Ferraz Leal, P. Rozycko, T. Snow and A. Washington, *Zenodo*, 2020, DOI: 10.5281/zenodo.3930098.
63. X. Yu, L. Chen, M. Zhang and T. Yi, *Chemical Society Reviews*, 2014, **43**, 5346-5371.
64. E. Fukushima and S. B. Roeder, *Experimental Pulse NMR: A Nuts and Bolts Approach*, Avalon Publishing, 1993.
65. A. C. Dona, G. Pages, R. G. Gilbert, M. Gaborieau and P. W. Kuchel, *Biomacromolecules*, 2009, **10**, 638-644.
66. A. C. Dona, G. Pages, R. G. Gilbert and P. W. Kuchel, *Carbohydr. Polym.*, 2011, **83**, 1775-1786.
67. F. S. Schoonbeek, J. H. v. Esch, R. Hulst, R. M. Kellogg and B. Feringa, *Chemistry : a European journal*, 2000, **6**, 2633-2643.
68. J. Teixeira, *J. Appl. Cryst.*, 1998, **21**, 781-785.
69. I. Livsey, *J. Chem. Soc., Faraday Trans. 2*, 1987, **83**, 1445-1452.
70. A. E. Whitten, S. Cai and J. Trewhella, *Journal of Applied Crystallography*, 2008, **41**, 222-226.